RESEARCH ARTICLE

The mitochondrial-related effect of the 905 nm photobiomodulation therapy on 50B11 sensory neurons

Luisa Zupin[1] 🔘 | Sergio Crovella[2] | Cadenaro Milena[1,3] | Egidio Barbi[1,3] | Fulvio Celsi[1]

[1]Institute for Maternal and Child Health IRCCS Burlo Garofolo, Trieste, Italy

[2]LARC - Laboratory Animal Research Center, Qatar University, Doha, Qatar

[3]Department of Medicine, Surgery and Health Sciences, University of Trieste, Trieste, Italy

Correspondence
Luisa Zupin, Institute for Maternal and Child Health IRCCS Burlo Garofolo, Trieste, Italy.
Email: luisa.zupin@burlo.trieste.it

Abstract

Photobiomodulation therapy (PBMT) is known as a complementary tool to alleviate pain sensation in patients, nevertheless, there is still a gap of knowledge on its mechanism of action, thus limiting its clinical employment. In this study, a possible molecular mechanism of the 905 nm PBMT (0.25 W/cm^2; 3, 6, 12, and 18 J/cm^2, 5 Hz) analgesic effect was tested on 50B11 cells, by investigating its impact

on mitochondria. A decrement of adenosine triphosphate was detected, moreover, an increment of total reactive oxygen species and mitochondrial superoxide anion was found after PBMT with all protocols tested. PBMT at 18 J diminished the mitochondrial membrane potential, and influenced mitochondrial respiration, decreasing the oxygen consumption rate. Finally, a decrement of extracellular signal-regulated kinase 1/2 phosphorylation was observed with the protocol using 12 J. Taken together these findings highlighted the intracellular effects, mainly correlated to mitochondrial, induced by 905 nm PBMT in sensory neurons, indicating the central role of this organelle in the cellular response to 905 nm near-infrared laser light.
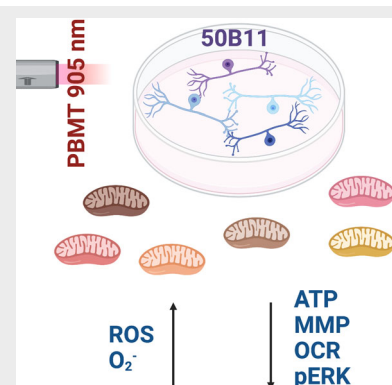
KEYWORDS
ERK signaling, mitochondria, photobiomodulation therapy, sensory neurons

1 | INTRODUCTION

Photobiomodulation therapy (PBMT) employs laser light to deliver photons on tissues in order to stimulate a cellular process defined as "photobiomodulation," an intracellular signaling cascade that from light reception by endogenous chromophores leads to several photophysical and photochemical events. As final outcome, PBMT acts on cellular metabolism and pathways, resulting in wound healing or inflammation's reduction as

few examples [1]. Moreover, different evidence highlights the beneficial impact of PBMT on pain reduction [2].

PBMT is already applied in different clinical settings due to its beneficial characteristics of biomodulation as well as for the noninvasiveness and the rapidity of painless application. Remarkably, for these reasons, PBMT treatment may be of particular interest for children, who may be scared by needle-related topical anesthesia practices or experience difficulties in oral assumption of drugs without specific pediatric formulations. Moreover, special needs children (with chronic complex severe conditions such as cerebral palsy or syndromic diseases) may be particularly vulnerable to painkiller adverse effects related to malnutrition, dehydration, muscle contractions, and other issues [3].

Among the most employed range of wavelengths, the near-infrared one (range 800–1000 nm) stands out for its beneficial effects on mitochondrial activity [1]. Indeed, cytochrome c oxidase (COX), a key enzyme of the complex IV of the mitochondrial respiratory chain, can be modulated by the NIR PBMT. COX presents two copper ion and two iron ion subunits that are supposed to be the cellular chromophores (photoreceptors) able to receive the photons and to activate the intracellular cascade induced by PBMT [4].

Among the possible cellular targets of PBMT, there are the sensory neurons whose free nerve endings in the skin can possibly sense the PBMT light. Several previous physiological studies explored the effect of PBMT on nerve conduction, highlighting that PBMT can lower the conduction velocity and decrease the amplitudes of action potentials. These effects result in the inhibition of nociception signaling in sensory neurons leading to pain relief and analgesia [5]. Chow et al. [6] observed that the 800 nm PBMT induced axonal varicosities rich in mitochondria and decremented mitochondrial membrane potential (MMP) in cultured rat dorsal root ganglion (DRG) sensory neurons, possibly blocking fast axonal flow and nociceptive signaling. Similarly, Holanda et al. [7] showed that 808 nm PBMT decreased the DRG neurons metabolism and caused the formation of varicosities in rat DRG. Our research group also performed PBMT experiments on murine DRG neurons. An increment of superoxide anion and of MMP was detected after 800 nm irradiation. On the other hand, calcium response towards capsaicin stimulus (a Transient Receptor Potential Vanilloid 1-ligand) was reduced by 970 nm wavelength. Both PBMT at 800 and 970 nm reduced adenosine triphosphate (ATP) production and increased reactive oxygen species (ROS) levels [8]. Further, we investigated PBMT effect on 50B11 immortalized rat sensory neurons cell line [9] differentiated upon treatment with forskolin. Both wavelengths boosted ATP level, hyperpolarized MMP and incremented ROS, while only 800 nm wavelength induced an increment of superoxide anion content. The 800 and 970 nm wavelength delivered singularly or in combination decreased the capsaicin-induced calcium flow [10].

Despite some highlights derived from the cellular studies above briefly described, the exact molecular mechanisms at the basis of these beneficial outcomes are not completely understood, causing some skepticism among scientists regarding the real PBMT benefits for relieving pain in patients. Moreover, few studies so far investigated PBMT consequences at the level of cellular physiology and signaling pathways.

Based on our previous results obtained in sensory neurons with the 800 and 970 nm NIR PBMT, in this study, we decided to deepen the knowledge on the effects of a NIR range different wavelength, the 905 one. The 905 nm PBMT was applied on 50B11 sensory neurons and its influence on mitochondria was investigated.

2 | MATERIALS AND METHODS

2.1 | 50B11 cell culture

In our experimental set, the immortalized rat sensory neuron 50B11 cell line was the neuronal model of nociceptive dorsal root ganglia neurons [9].

The cells were maintained in Neurobasal medium (21103049, Gibco, Thermo Fisher Scientific, Waltham, Massachusetts) with 10% of fetal bovine serum (Euroclone, Pero, Milan, Italy), 2% B27 (Life Technologies), 0.22% glucose (Merck, Readington Township, New Jersey), 0.2 mM glutamine (Euroclone) and penicillin/streptomycin 100 U/mL (Euroclone).

For the experiments poly-D-lysine coated (0.1 mg/mL, P6507, Merck) optical black 96 multiwell plates (Greiner Bio-One, Kremsmünster, Austria) were employed; 30,000 cells/well were seeded on the plates and after 24 h the medium was completely changed with fresh medium composed by Neurobasal medium without phenol red (12348017, Gibco), 0.2% of fetal bovine serum (Euroclone, Pero, Milan, Italy), 2% B27 (Life Technologies), 0.22% glucose (Merck), 0.2 mM glutamine (Euroclone) and penicillin/streptomycin 100 U/mL Penicillin/Streptomycin (Euroclone), supplemented with 75 μM forskolin (F6886, Merck) to induce the differentiation and maturation of 50B11 cells.

2.2 | Photobiomodulation protocols

The photobiomodulation was carried out with a K-Laser Cube series (K-laser d.o.o., Sežana, Slovenia) by using the zoom tip set to uniformly cover the spot area (1 cm^2). Four protocols employing a 905 nm wavelength were tested as reported in Table 1.

TABLE 1 Photobiomodulation therapy Protocols (1–4) employed in this study.

	Protocol 1	Protocol 2	Protocol 3	Protocol 4
Wavelength	905 nm			
Irradiance	0.25 W/cm^2 (output power 0.6 W)			
Fluence	3 J/cm^2	6 J/cm^2	12 J/cm^2	18 J/cm^2
Spot size	1 cm^2			
Pulsed modality	5 Hz with 50% duty cycle			

2.3 | Mitochondria assessment

2.3.1 | 3-(4,5-Dimethylthiazol-2-yl)-2,5-diphenyltetrazolium bromide assay

One hour after irradiation the reduction of 3-(4,5-dimethylthiazol-2-yl)-2,5-diphenyltetrazolium bromide (MTT; 1.2 mM final concentration, MTT, M6494, Life Technologies, Thermo Fisher Scientific) by NADPH-dependent cellular oxidase was assessed to determine the possible photoeffect of PBMT on 50B11 viability and metabolism. After 2 h the formazan was dissolved in 10% sodium dodecyl sulfate/HCl 0.01 M overnight and the absorbance read at 595 nm on the GloMax-Multi Detection System (Promega, Fitchburg, Wisconsin).

2.3.2 | ATP determination

Immediately, 1, 4, or 24 h after irradiation, ATP was measured with the ATP determination kit (A22066, Life Technologies, Thermo Fisher Scientific) at the GloMax-Multi Detection System (Promega) and normalized on protein concentration by using bovine serum albumin as standard (Bradford assay, Bio-Rad, Hercules, California).

2.3.3 | Oxidative stress

Immediately after PBMT, oxidative stress was evaluated with the Cell Rox reagent to evaluate the total ROS content (5 μM at 37°C for 1 h, C10444, Life Technologies, Thermo Fisher Scientific) and with the MitoSOX staining to estimate the superoxide anion generation, specifically produced by mitochondria metabolism (10 μM at 37°C for 1 h, M36008, Life Technologies, Thermo Fisher Scientific).

The fluorescences were read on the Cytation 5 Cell Imaging Multimode Reader (Biotek, Winooski, Vermont) and and normalized on the protein concentration measured with Bradford protein assay (Bio-Rad).

Antimycin A (J63522.MA, Thermo Fisher Scientific), an inhibitor of ATP synthase (5 μM, 1 h) was employed as control.

The activity of the superoxide dismutase (SOD) was assessed by the SOD Colorimetric Activity Kit (EIASODC, Thermo Fisher Scientific) according to the manufacturer's instructions, 0, 1, and 4 h from irradiation.

MMP was determined with the JC-1 probe (staining: 5 μM at 37°C for 1 h, T3168, Life Technologies, Thermo Fisher Scientific). The fluorescence was read at the Cytation 5 Cell Imaging Multimode Reader (Biotek, Winooski, Vermont) and the results were reported as red (590 nm) to green (525 nm) fluorescence intensity ratio.

Moreover, representative pictures of each condition were captured at the Cytation5 Cell Imaging Multimode Reader (Biotek).

Carbonyl cyanide 3-chlorophenylhydrazone (CCCP, C2759 Merck), an uncoupler of oxidative phosphorylation (5 μM, 1 h) was employed as control.

2.3.4 | Mitochondrial respiration

Mitochondrial respiration was tested with the Agilent MitoXpress Xtra Oxygen Consumption Assay (Agilent Technologies, Santa Clara, California) that allowed the real-time measurement of extracellular oxygen consumption rates (OCR) determined by cellular respiration and mitochondrial functionality. Briefly, the fluorescent probe is quenched by O_2; therefore, the fluorescence signal is inversely proportional to the extracellular O_2 in the sample.

After irradiation, the cells were loaded with the dye and overlaid with a drop of mineral oil, then after 15 min of re-equilibration in the incubator at 37°C, 5% CO_2 the changes of the fluorescence were monitored for 90 min at the Cytation 5 Cell Imaging Multimode Reader (Biotek, excitation at 340 nm, emission at 650 nm). The dual read time-resolved fluorescence was employed for the analysis and the fluorescence was normalized on the signal of blank wells (without cells). Lifetime was computed and used to calculate the OCR.

CCCP (5 μM, 1 h) was employed as control.

2.4 | Activation of extracellular signal-regulated kinase

The amount of extracellular signal-regulated kinase (ERK) and phosphorylated ERK was analyzed by western blot. UO126, an inhibitor of ERK phosphorylation (10 μM for 1 h Cell Signaling Technologies, CST, Leiden, The Netherlands) was employed as technical control.

Briefly, 50B11 (180,000 cells/well) were seeded on 48 multiwells plate and after irradiation lysed in 25 μL of RIPA lysis buffer (89901, Thermo Fisher Scientific) plus inhibitor of phosphatase and phosphorylase (Halt Protease and Phosphatase Inhibitor Cocktail 78440, Thermo Fisher Scientific). After protein normalization (Bradford protein assay, Bio-Rad), the samples were loaded for the electrophoresis separation on the 4%–20% Mini-PROTEAN TGX Precast Protein Gels (Bio-Rad) and then transferred to Trans-Blot Turbo Mini 0.2 μm Nitrocellulose membrane (Bio-Rad) by using the Trans-Blot Turbo Transfer System (Bio-Rad).

Membranes were then incubated in the I-Bind device by employing the I-Bind card and I-Bind solution kit (Thermo Fisher Scientific) following manufacturer's instructions. Primary antibody for phosphorylated form of ERK (phospho-p44/42 MAPK, Erk1/2, Thr202/204, D13.14.4E XP, 4370S, 1:1000 Cell Signaling Technologies, CST, Leiden, The Netherlands) was used, by utilizing heat shock protein 90 (HSP90) as internal calibrator (1:1000, sc-13 119, Santa Cruz Biotechnologies, Dallas, Texas) and by employing horseradish peroxidase-conjugated secondary antibodies (7074S, 7076S, 1:1000, CST, Leiden, The Netherlands). The membranes were then developed with SuperSignal West Pico PLUS Chemiluminescent Substrate (34577, Thermo Fisher Scientific) at the Chemidoc instrument (Bio-Rad). After images' acquisition, the membranes were stripped and reprobed with a primary antibody for ERK (p44/42 MAPK, Erk1/2, 137F5, 4695S, 1:500, Cell Signaling Technologies, Leiden, The Netherlands). The ratio between the phosphorylated form of ERK and ERK was used in the statistical analysis.

2.5 | Statistical analysis

The Kruskal–Wallis test corrected for multiple comparisons with Dunn's test and two-way ANOVA (analysis of variance) corrected for Holm–Šídák's multiple comparisons test were employed to compare the not irradiated cells (not treated [NT]) with the other experimental conditions on the R software [11], considering statistically significant all values of $p < 0.05$.

3 | RESULTS

Based on our previous experience on the effect of PBMT in the near-infrared range [8, 10] four protocols employing different energies (see Table 1 for the details) were selected and tested on the 50B11 cells.

MTT test was used as a first screening assay to evaluate the possible phototoxicity of PBMT protocols: no statistically significant differences were found between the treated and NT cells (data not shown).

Five different tests were used to determine the impact of PBMT on mitochondrial functionality.

The level of ATP, a key energy molecule produced by mitochondria, was significantly decreased after 1 h from irradiation by employing the protocols 2,3,4 that presented higher fluences (6, 12, and 18 J). A trend of the classical biphasic dose response was observed being the protocol 3 (12 J) the strongest in its reduction effect (Kruskal–Wallis with Dunn's post hoc test: Protocol 2 vs. NT cells, p-value = 0.01; Protocol 3 vs. NT, p-value = 0.007; Protocol 4 vs. NT, p-value = 0.01; Figure 1A). The measurement of ATP immediately after PBMT showed no differences among irradiated and not irradiated cells, similarly, ATP content was also measured at 4 and 24 h from the irradiation but the ATP levels returned to the basal level and were similar to the NT cells (data not shown). When looking at the oxidative stress, an increment of total ROS as well as of the superoxide anion, a specific product of mitochondrial metabolism, was observed with all the protocols (ROS: Kruskal–Wallis with Dunn's post hoc test: Protocol 1 vs. NT, p-value = 0.0001; Protocol 2 vs. NT, p-value = 0.02; Protocol 3 vs. NT, p-value = 0.02, Protocol 4 vs. NT, p-value = 0.02; Figure 1B; superoxide anion: Kruskal–Wallis with Dunn's post hoc test: Protocol 1 vs. NT, p-value = 0.02; Protocol 2 vs. NT, p-value = 0.005, Protocol 2 vs. NT, p-value = 0.04; Protocol 4 vs. NT, p-value = 0.02; Figure 1C). Nevertheless, these ROS levels were not toxic for the cells since the activity of the SOD was not induced by the irradiation (data not shown).

MMP was also assessed. A statistically significant depolarization was induced by the Protocol 4 employing 18 J of energy (Kruskal–Wallis with Dunn's post hoc test: Protocol 4 vs. NT, p-value = 0.02; Figure 2S). Figure 2 illustrated also some representative images of the PBMT effect on MMP.

The same PBMT parameters were also efficacious in inhibiting the mitochondrial respiration evaluated as OCR (two-way ANOVA with Holm–Šídák's multiple comparisons test, Protocol 4 vs. NT, p-value = 0.01; Figure 3).

Finally, the ERK pathway was studied analyzing the phosphorylation of ERK: a decrement of the
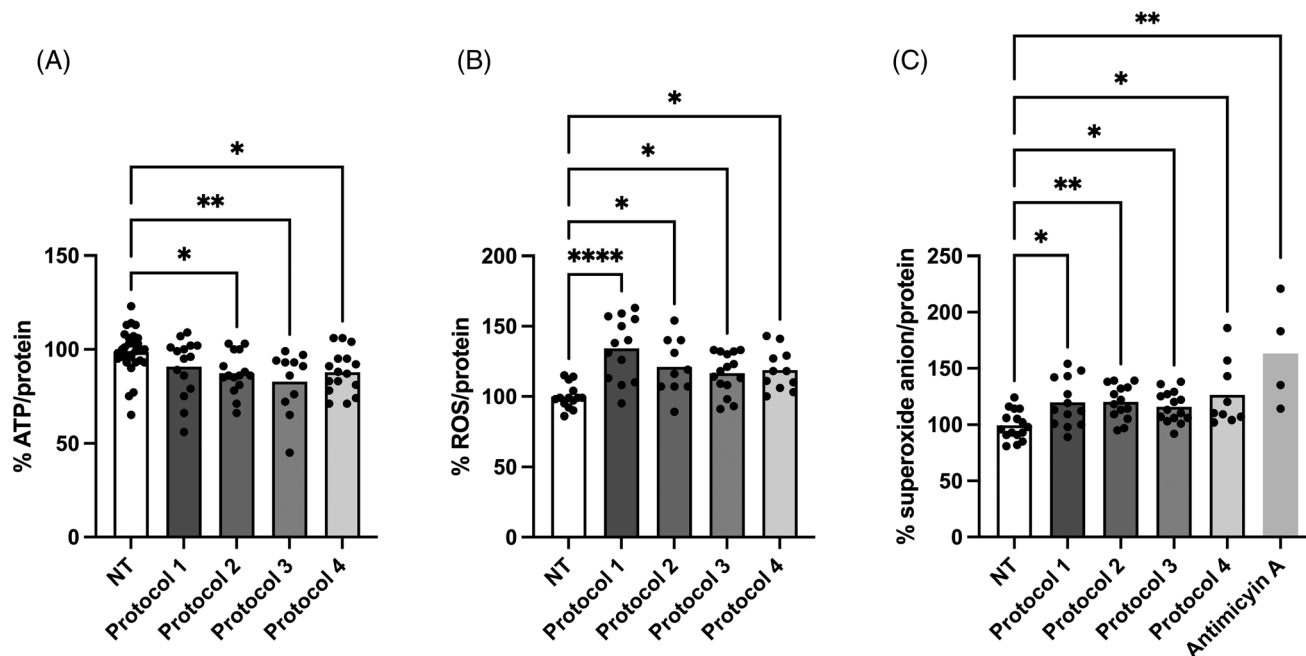
FIGURE 1 Photobiomodulation therapy (PBMT) 905 nm effect on 50B11 sensory neurons. (A) adenosine triphosphate (ATP) assay (ATP content normalized on protein concentration) after 1 h from PBMT in 50B11 cells. (B) Reactive oxygen species (ROS; normalized on protein concentration) after 15 min from PBMT in 50B11 cells. (C) Superoxide anion (normalized on protein concentration) after 15 min from PBMT in 50B11 cells. The data of each PBMT treatment (Protocols 1–4, Table 1) are reported as percentage respect to the not irradiated cells (designed as not treated [NT]). The statistically significant results from Kruskal–Wallis test with post hoc Dunn's multiple comparisons test were reported (****p-value < 0.0001; **p-value < 0.01; *p-value < 0.05).

phosphorylation was found with the Protocol 3 respect to the not irradiated cells (Kruskal–Wallis with Dunn's post hoc test: Protocol 3 vs. NT, p-value = 0.01; Figure 4).

4 | DISCUSSION

This study shows that PBMT at 905 nm can influence mitochondrial functionality; indeed, by analyzing different mitochondria-related parameters a significant impact of PBMT on mitochondria was detected.

A decrement of ATP level, a key energetic product, was found after 1 h from irradiation. Moreover, an increment of oxidative stress was also displayed, being both total ROS and superoxide anion incremented after PBMT with all protocols tested. Only PBMT protocol at 18 J of energy (Protocol 4) affected the MMP decrementing it after 15 min from irradiation, and the same protocol negatively influenced the mitochondrial respiration, decreasing the OCR.

All these tests highlighted the mitochondrial involvement in the response to the 905 nm light in sensory neurons.

The observed ATP decrement is in line with the results obtained in DRG murine neurons [8], but not with that noted in 50B11 cells in our previous study [10]

in which we used different protocols employing the 800 and 970 nm of wavelengths. The decrement of ATP was also in line with the study by Holanda et al. [7] showing a reduction of metabolism in 830 nm irradiated rat DRG neurons. ATP is a key energetic molecule for cellular functionality and in sensory neurons is fundamental for the generation of action potential through Na+/K+ ATPase and nociceptive signaling. Moreover, ATP is also a neurotransmitter implicated in neuronal sensitization through the P2X receptors and neuropathic pain [12]. Nevertheless, the decrement observed resolved after 4 h and also at 24 h the ATP level remained at the same level of the not irradiated cells, indicating that the PBMT was transient and not maintained over the observational period. Moreover, the measurement of ATP immediately after PBMT did not show statistically significant differences, suggesting that the PBMT influence on ATP production took some time (1 h) to be effective.

The present data confirmed the effects that were formerly detected with 800 and 970 nm protocols for total ROS, while the increment of superoxide anion was previously induced only by the 800 nm wavelength and not by the 970 one [10]. Superoxide anion is mainly a byproduct of mitochondrial metabolism generated through the one-electron reduction of O_2 at the electron transport chain,
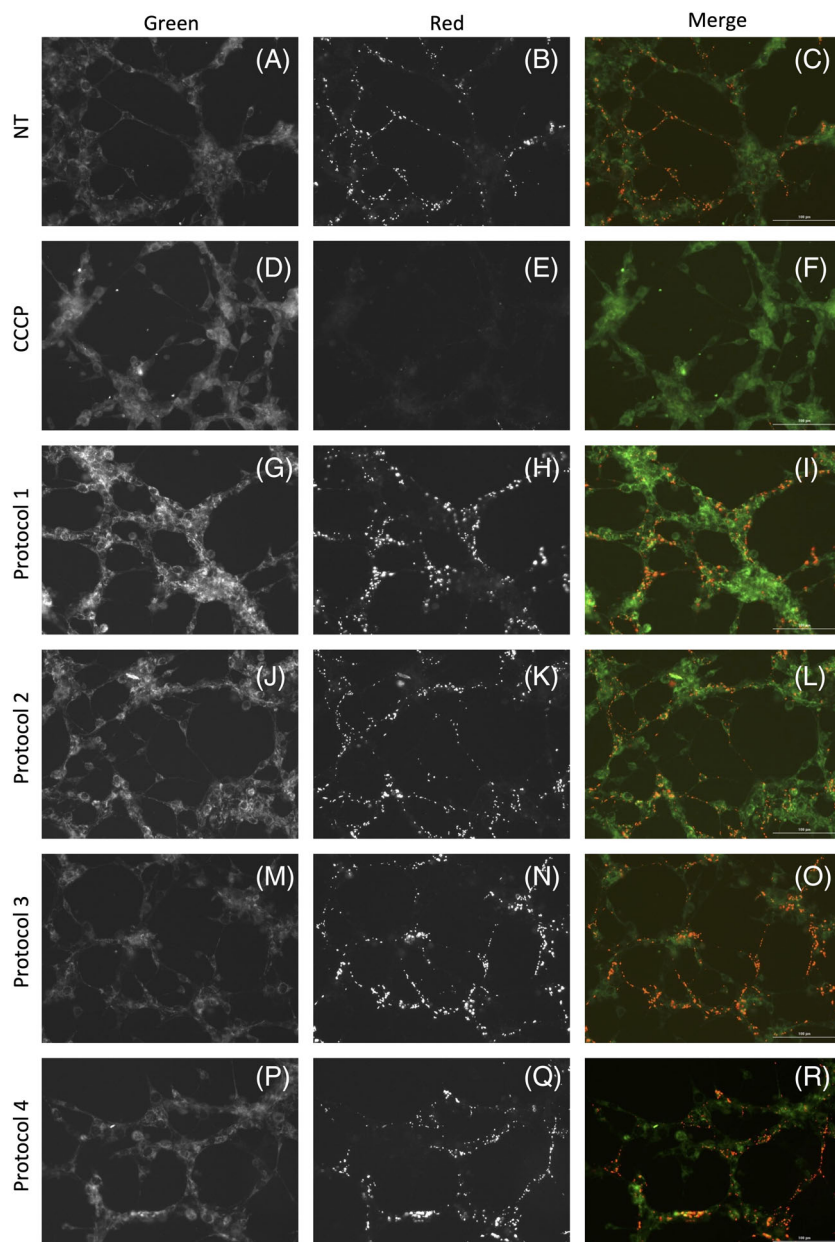
FIGURE 2 Mitochondrial membrane potential (MMP) after 15 min from photobiomodulation therapy (PBMT) in 50B11 cells. Representative images of MMP signal in the irradiated and not irradiated cells and in carbonyl cyanide 3-chlorophenylhydrazone (CCCP)-treated 50B11. First column: emission at 525 nm—green displayed in gray scale; Second column: emission at 590 nm—red displayed in gray scale; Third column: merged channels, in green—emission at 525 nm and red emission at 590 nm. (A–C) not treated (NT) cells; (D–F) CCP-treated cells; (G–I) Protocol 1; (J–L) Protocol 2; (M–O) Protocol 3; (P–R) Protocol 4. Scale bar 100 μM. (S) The data of each PBMT treatment (Protocols 1–4, Table 1) are reported as percentage of Red/Green fluorescence emission of JC1 probe and normalized towards not irradiated cells (designed as NT). The statistically significant results from Kruskal–Wallis test with post hoc Dunn's multiple comparisons test were reported (****p–value < 0.0001, *p-value < 0.05).
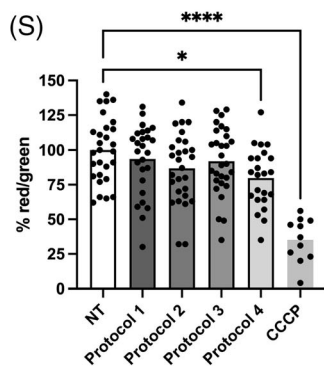
it is a highly active oxidizing moieties and it is rapidly converted in H_2O_2 by the SOD [13]. Nevertheless, the PBMT induction of superoxide anion detected was not related to an increment of the SOD activity, suggesting that the increment achieved was within a physiologic range.
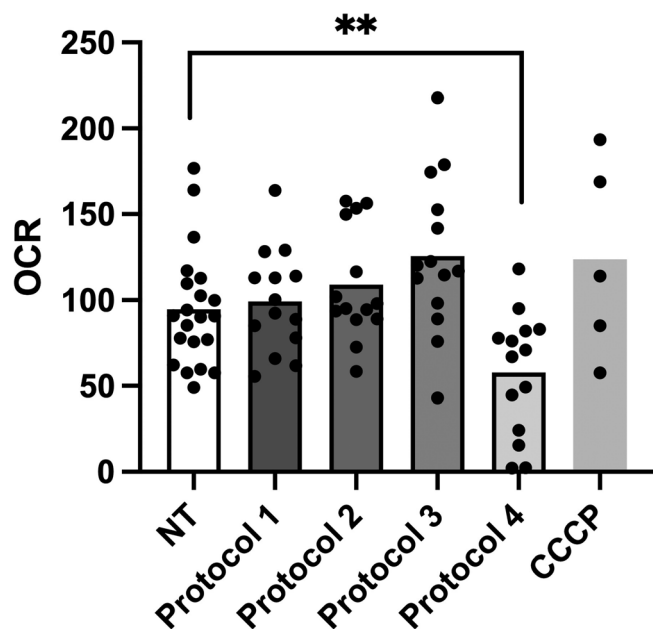
FIGURE 3 Oxygen consumption rate (OCR) after 15 min from photobiomodulation therapy (PBMT) in 50B11 cells. The data of each PBMT treatment (Protocols 1–4, Table 1) are reported as percentage respect to not irradiated cells (designed as not treated [NT]). The statistically significant results from two-way ANOVA corrected for Holm–Šídák's multiple comparisons test were reported (**p-value < 0.01).

Only the longer protocol (18 J, 120 s of irradiation) significantly impacted on MMP inducing a depolarization of the potential correlated to an inhibition of the mitochondrial respiration measured as OCR. An MMP decrement was previously detected by Chow et al. [6] in DRG axons after 5 min with 830 nm irradiation over a period of 30 min, as well as in the cell bodies, but only after 20 min from PBMT. Intriguingly, Chow et al. [6] observed that PBMT promoted the appearance of varicosities in the axons, that were rich in beta tubulin and mitochondria, in which the researcher observed in live imaging also the decrement of MMP. These findings suggested that PBMT induced microtubules disruption at varicosity level, leading to the inhibition of the mitochondria trafficking between the soma and the synapse; moreover, these movements were important to replenish also the ATP-depleted mitochondria at the axon terminals. All these activities are essential for neurons to generate and restore axon potential as well as for the delivery of neurotransmitters [14], intriguingly at the same time the varicosities were described as important neuroprotective features [15]. In our study, varicosities were not clearly identified, but the employment of an immortalized cell line respect to primary DRG neurons could account for these divergences.
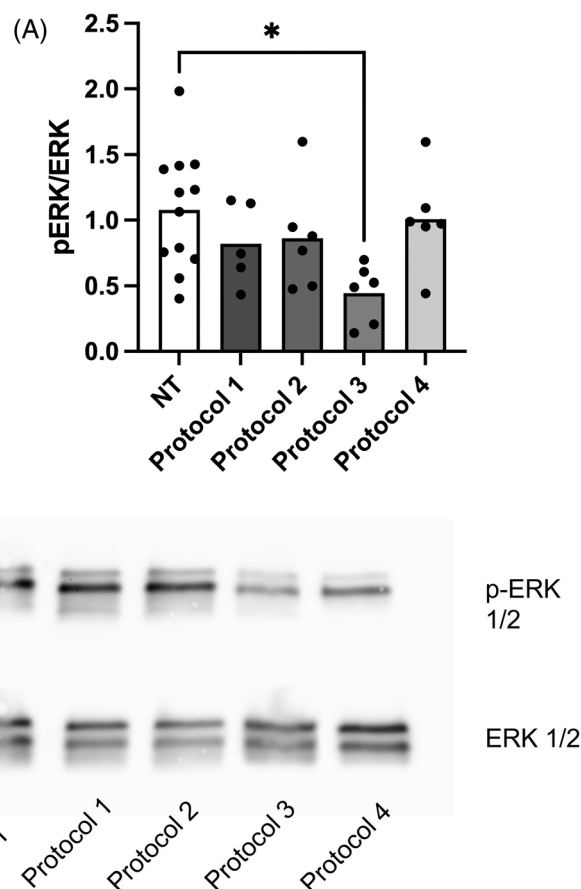

FIGURE 4 (A) The ratio of phosphorylated extracellular signal-regulated kinase (ERK) to total ERK content after 15 min from photobiomodulation therapy (PBMT) in 50B11 cells. The data of each PBMT treatment (Protocols 1–4, Table 1) and not treated (NT) cells were shown. The statistically significant results from Kruskal–Wallis with Dunn's post hoc test were reported (*p-value < 0.05). (B) Exemplificative western blot image, showing a marked reduction of ERK phosphorylation (p-ERK) 1/2 using Protocol 3, while levels of total ERK1/2 remain unchanged between treatment.

MMP depolarization was in disagreement with our previous reports but it can be explained by the different wavelengths employed in the former studies [8, 10].

Finally, the decrement of ERK1/2 phosphorylation was observed with the Protocol 3 using 12 J. ERK pathways plays multiple role in DRG neurons and its phosphorylation is activated in neurons after noxious stimuli, while its inhibition suppress painful sensation so representing an appealing target for analgesic research [16]. Very interestingly, these observations are in line with our findings, highlighting a decrease of phosphorylated ERK after PBMT, so potentially representing an approach to block pain signaling pathways. Moreover, PBMT at 904 nm was able to decrement the activation DRG in streptozotocin treated rats [17].

Taken together the findings here reported highlighted the intracellular effects of the 905 nm PBMT in sensory neurons. Indeed, different mitochondrial-related parameters were influenced by 905 nm PBMT, as ATP level, ROS generation, superoxide anion induction, MMP depolarization, inhibition of mitochondrial respiration, and ERK dephosphorylation.

This specific wavelength, the 905 nm one, was previously employed in PBMT clinical settings, and it has been considered as a promising treatment for major knee osteoarthritis [18], temporomandibular disorders [19], neck chronic myofascial pain [20], lateral elbow tendinopathy [21], lateral epicondylitis [21] in adults, but also in oncologic children as a preventive strategy to block the development of oral mucositis [22]. So, new insides in the molecular mechanisms of 905 nm PBMT, as those described in this work, will be useful to promote its clinical employment. Indeed, PBMT, apart from the beneficial outcomes of the photon's delivery, presents several advantageous features, such as the noninvasiveness, the rapidity of painless treatments, resulting in an effective approach to treat fragile subjects as sick children.

AUTHOR CONTRIBUTIONS

Luisa Zupin participated in the study design and conception, performed the experiments and contributed to the writing of the article. Cadenaro Milena, Sergio Crovella, and Egidio Barbi critically revised the article. Fulvio Celsi participated in the study design and conception, performed the experiments, and contributed to the writing of the article.

CONFLICT OF INTEREST STATEMENT

The authors declare no conflict of interest.

DATA AVAILABILITY STATEMENT

Data available on request from the authors.

ORCID

Luisa Zupin https://orcid.org/0000-0001-5886-9129

REFERENCES

[1] L. F. de Freitas, M. R. Hamblin, *IEEE J Sel Top Quantum Electron* **2016**, *22*, 348.

[2] R. T. Chow, P. J. Armati, *Photomed Laser Surg* **2016**, *34*, 599.

[3] M. Massaro, S. Pastore, A. Ventura, E. Barbi, *Eur J Pediatr* **2013**, *172*, 9.

[4] G. E. Glass, *J Plast Reconstr Aesthet Surg* **2021**, *74*, 1050.

[5] R. Chow, P. Armati, E.-L. Laakso, J. M. Bjordal, G. D. Baxter, *Photomed Laser Surg* **2011**, *29*, 365.

[6] R. T. Chow, M. A. David, P. J. Armati, *J Peripher Nerv Syst* **2007**, *12*, 28.

[7] V. M. Holanda, M. C. Chavantes, X. Wu, J. J. Anders, *Lasers Surg Med* **2017**, *49*, 516.

[8] L. Zupin, G. Ottaviani, K. Rupel, M. Biasotto, S. Zacchigna, S. Crovella, F. Celsi, *J Biophotonics* **2019**, *12*, e201900043.

[9] W. Chen, R. Mi, N. Haughey, M. Oz, A. Höke, *J Peripher Nerv Syst* **2007**, *12*, 121.

[10] L. Zupin, E. Barbi, R. Sagredini, G. Ottaviani, S. Crovella, F. Celsi, *J Biophotonics* **2021**, *14*, e202000347.

[11] R Core Team. The R Project for Statistical Computing. **2023**. http://www.R-project.org.

[12] T. H. Tam, M. W. Salter, *Purinergic Signalling* **2021**, *17*, 49.

[13] N. Gamper, L. Ooi, *Antioxid Redox Signaling* **2015**, *22*, 486.

[14] T. Nakata, S. Terada, N. Hirokawa, *J. Cell Biol.* **1998**, *140*, 659.

[15] A. D. Liebert, R. T. Chow, B. T. Bicknell, E. Varigos, *J Exp Neurosci* **2016**, *10*, JEN.S33444.

[16] M. Kondo, I. Shibuta, *J Oral Sci.* **2020**, *62*, 147.

[17] W. F. Vieira, K. F. Malange, S. F. de Magalhães, J. B. P. Lemes, G. G. dos Santos, C. M. Nishijima, A. L. R. de Oliveira, M. A. da Cruz-Höfling, C. H. Tambeli, C. A. Parada, *Sci. Rep.* **2022**, *12*, 16730.

[18] M. B. Stausholm, I. F. Naterstad, J. Joensen, R. Á. B. Lopes-Martins, H. Sæbø, H. Lund, K. V. Fersum, J. M. Bjordal, *BMJ Open* **2019**, *9*, e031142.

[19] H. Ren, J. Liu, Y. Liu, C. Yu, G. Bao, H. Kang, *J Oral Rehabil* **2022**, *49*, 138.

[20] A. Gur, A. J. Sarac, R. Cevik, O. Altindag, S. Sarac, *Lasers Surg Med* **2004**, *35*, 229.

[21] J. M. Bjordal, J. Joensen, C. Couppe, A. E. Ljunggren, A. Stergioulas, M. I. Johnson, *BMC Musculoskelet Disord* **2008**, *9*, 75.

[22] S. V. Moskvin, A. A. Khadartsev, *BioMedicine.* **2020**, *10*, 1.

How to cite this article: L. Zupin, S. Crovella, C. Milena, E. Barbi, F. Celsi, *J. Biophotonics* **2023**, *16*(9), e202300130. https://doi.org/10.1002/jbio.202300130